

RSC Advances



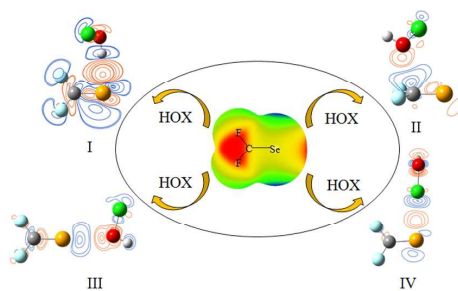
This is an *Accepted Manuscript*, which has been through the Royal Society of Chemistry peer review process and has been accepted for publication.

Accepted Manuscripts are published online shortly after acceptance, before technical editing, formatting and proof reading. Using this free service, authors can make their results available to the community, in citable form, before we publish the edited article. This *Accepted Manuscript* will be replaced by the edited, formatted and paginated article as soon as this is available.

You can find more information about *Accepted Manuscripts* in the [Information for Authors](#).

Please note that technical editing may introduce minor changes to the text and/or graphics, which may alter content. The journal's standard [Terms & Conditions](#) and the [Ethical guidelines](#) still apply. In no event shall the Royal Society of Chemistry be held responsible for any errors or omissions in this *Accepted Manuscript* or any consequences arising from the use of any information it contains.

TOC



The complexes between F_2CSe and HOX have been investigated to unveil the influence of F and Se substitution.

**Influence of F and Se substitution on the structures,
stabilities and nature of the complexes between F₂CSe and
HOX (X = F, Cl, Br, and I)**

Xin Guo, Qingzhong Li*, Bo Xiao, Xin Yang, Wenzuo, Li, Jianbo Cheng

*The Laboratory of Theoretical and Computational Chemistry, School of Chemistry
and Chemical Engineering, Yantai University, Yantai 264005, People's Republic of
China*

Corresponding author:

Qingzhong Li Dr

The Laboratory of Theoretical and Computational Chemistry

School of Chemistry and Chemical Engineering

Yantai University

Yantai 264005

People's Republic of China

Tel. (+086) 535 6902063

Fax. (+086) 535 6902063

E-mail: liqingzhong1990@sina.com

Abstract

Ab initio MP2/aug-cc-pVTZ calculations have been performed to identify local minima on the $F_2CSe-HOX$ ($X = F, Cl, Br, \text{ and } I$) potential surface, to characterize the types of interactions which stabilize the complexes found at these minima, and to evaluate their relative stabilization. Four types of structures are found for each complex except the HOF one. The $Se\cdots H$ hydrogen-bonded complexes (I) are accompanied with a secondary $X\cdots F$ interaction. The structure II is jointly connected with a tetrel bond and a $X\cdots Se$ interaction. The structures III and IV are stabilized by a chalcogen bond and a halogen bond, respectively. I has a little dependence in stabilization on the nature of X atom, while II, III, and IV become more stable with the increase of X atomic mass. The chalcogen-bonded complexes are least stable, the halogen-bonded complexes are more stable than the tetrel-bonded ones, and the hydrogen-bonded complex is weaker than the halogen-bonded one in the HOI complex but stronger in other complexes. The formation of these interactions has been understood by means of molecular electrostatic potentials and orbital interactions. The electrostatic energy is dominant in the complexes I and IV although the polarization and dispersion contributions are also important, while the dispersion energy is comparable with the electrostatic contribution in the complexes II and III.

Keywords: Hydrogen bond; Tetrel bond; Chalcogen bond; Halogen bond; F_2CSe

1. Introduction

The physicochemical and spectroscopic properties of X_2CY ($X = H, F, Cl, Br; Y = O, S, Se$) have attracted a great deal of attention for many decades.¹⁻³ It is because such studies are beneficial to understand the effects of chalcogen and halogen substitutions that play a significant role in chemistry and biochemistry.^{4,5} For instance, F_2CO and Cl_2CO have been found to be the primary products in the photodecomposition reaction of methinehalide by the circumstance of oxygen.⁶ The organoselenium chemistry has rapidly developed since selenium was demonstrated to be an important factor in understanding the biological functions of several selenoproteins.⁷ On the one hand, the compounds with a selenocarbonyl group have been taken as composition units in organic syntheses and as important intermediates involved in the synthesis of selenium-containing molecules.⁸⁻¹⁰ Also it was shown that selenoformaldehyde (H_2CSe) and its corresponding dihalogen derivatives are related to the systems of biological importance.^{1,11,12}

Hypohalous acids (HOX , $X = \text{halogen}$) are powerful oxidizing agents with diverse action sites and significant chemical activities. However, their chemical instability makes it difficult to study their properties experimentally. Thus, theoretical methods have usually been used to study the complexes of hypohalous acids with themselves¹³ and other molecules.¹⁴⁻¹⁸ Hypohalous acids are also important in field of atmospheric chemistry because they are plentifully formed in the atmosphere by the reactions between X and OH radicals. For instance, hypobromous acid has a key function in the catalytic processes in depletion of stratospheric ozone.¹⁹ More importantly,

hypohalous acids are closely related to protein pharmaceutical²⁰ and infectious diseases.²¹ Hypochlorous and hypobromous acids are antimicrobial oxidants produced by innate immune cells.²² Moreover, hypochlorous can awaken the enzymatic activity during the oxidation of lysozyme.²³

In this paper, we perform a research for the complexes of F_2CSe and HOX ($X = F, Cl, Br, \text{ and } I$) by quantum chemical calculations. The first interest is if their structures can be stabilized by hydrogen bond, halogen bond, chalcogen bond, or tetrel bond? Our second attention is the effect of these interactions on the structures and properties of the complexes. Thirdly, it is urgent to unveil the origin of these interactions. To our best knowledge, the complexes of F_2CSe and hypohalous acids have not been investigated both theoretically and experimentally. This research gap pushes us to research the structures, properties, and nature of these complexes. We think that this work could be vital to deepen understanding of the interaction mechanism between them with potential significance in biology and atmospheric chemistry.

2. Theoretical calculations

The geometries of binary systems were optimized at the MP2 level with the aug-cc-pVTZ basis set for all atoms except iodine atom. The aug-cc-pVTZ-PP basis set involving pseudo potential was adopted for the iodine atom to account for relativistic effects. Harmonic frequency calculations were computed at the same level to confirm that all structures correspond to the true minima on the potential energy surfaces. Interaction energies were computed as the difference between the energy of

the complex and the sum of the energies of the two optimized monomers. Interaction energies were corrected for basis set superposition error (BSSE) using the counterpoise procedure proposed by Boys and Bernardi.²⁴ All calculations were carried out with the Gaussian 09 program.²⁵

Molecular electrostatic potentials (MEPs) at the 0.001 electrons Bohr⁻³ isodensity surfaces were calculated with the Wave Function Analysis-Surface Analysis Suite (WFA-SAS) program²⁶ at the MP2/aug-cc-pVTZ level. The MP2/aug-cc-pVTZ wave functions as input were applied to obtain the topological parameters using AIM2000 software²⁷ as well as the electron density shifts plotted by Multiwfn package.²⁸ NBO calculations²⁹ were performed to analyze orbital interactions at the HF/aug-cc-pVTZ level via the procedures contained within Gaussian 09. The interaction energy was decomposed using the GAMESS program³⁰ with the LMOEDA method³¹ at the MP2/aug-cc-pVTZ level.

3. Results and discussion

3.1. MEPs of F₂CSe and hypohalous acids

It was known that F₂CSe can act as both the Lewis acid and base to participate in different types of intermolecular interactions.³² To have a good understanding for the interaction sites in F₂CSe, its molecular electrostatic potential (MEP) map is plotted in Fig. 1. Blue and red regions represent the negative and positive MEPs, respectively. Clearly, two red regions are observed in F₂CSe. One red area is perpendicular to the plane composed of the C and two F atoms and the other one is at the outer surface of the Se atom along the C=Se axis. The former belongs to the π -hole, while the latter is called

σ -hole. The π -hole (1.164 eV) displays a larger positive MEP than the σ -hole (0.808 eV). Simultaneously, two negative regions with the value of -0.423 eV are located at both sides of the Se atom within the molecular plane of F₂CSe, corresponding to the lone-pair electrons on the Se atom. Therefore, F₂CSe provides not only the Lewis acid sites (the σ -hole and π -hole) to the Lewis base but also the Lewis base sites to the Lewis acid.

Fig. 2 is the MEP maps of hypohalous acids. Actually, they have been studied in the previous studies.^{18,33} Also two types of positive MEPs are found in HOX. One corresponds to the acidic proton and the other is associated with the σ -hole on the halogen atom except F. In addition, the surfaces of the oxygen and halogen atoms exhibit blue areas with negative MEPs. The most positive and negative MEPs in HOX (X = F, Cl, Br, and I) are collected in Table 1. With the increase of the halogen atomic size, the positive MEP on the H atom becomes smaller, whereas that on the σ -hole of the halogen atom is larger. This order is related to the electronegativity of halogen atom. Moreover, the former value is bigger than the latter one in all hypohalous acid molecules, indicating that the acidic proton is a stronger Lewis acid than the halogen atom. For the same reason, the negative MEP on the oxygen atom becomes more negative with the increase of halogen atomic mass. However, the negative MEP on the halogen atom is smaller in the same order. The above analyses for the MEPs of HOX indicate that this molecule is multi-functional molecules with two Lewis acid sites (H and X) and two Lewis base sites (O and X).

3.2. Geometries and frequency shifts

According to the electrostatic potentials of F_2CSe and HOX , we have obtained four types of complexes for each hypohalous acid except HOF , for the latter molecule three types of complexes are found. It should be pointed out that there also are other types of structures for the complexes of F_2CSe and HOX . However, they are less stable than the structures shown in Fig. 3 or are second-order saddle points.

In $F_2CSe-HOX-I$, the acidic H atom in HOX points to the lone-pair electron on the Se atom in F_2CSe . However, the H-O bond has a small deviation from the molecular plane of F_2CSe . In the initial optimization of $F_2CSe-HOX-I$, we designed the planar structure of complex with a hydrogen bond and the X atom being on opposite side of F atom in F_2CSe to reduce the repulsion interaction between the X atom of HOX and the F atom of F_2CSe . Unluckily, this planar structure is unstable with one imaginary frequency and becomes the nonplanar structure shown in Fig. 3 in the re-optimization process. With the increase of X atomic mass of HOX (X = Cl, Br, and I), the $Se\cdots H$ hydrogen bond shows a longer binding distance and a weaker strength, consistent with the positive MEP on the H atom of HOX . However, $F_2CSe-HOF-I$ has the longest binding distance, which is inconsistent with the largest MEP on the H atom of HOF . This abnormal result was also found in the hydrogen-bonded complexes of HOX and some nitrogenated bases (NH_3 , N_2 , and HCN).³⁴ Interestingly, there is an attractive interaction between the X atom of HOX and the F atom of F_2CSe , characterized with a $X\cdots F$ bond critical point (BCP) in Fig. 4. Furthermore, with the increase of X atomic mass, the $X\cdots F$ interaction is stronger, evidenced by the greater of electron density at the $X\cdots F$ BCP in Fig. 4. This attractive

interaction has an important effect on the nonplanar structure of $F_2CSe-HOX-I$, although it is weak with a long binding distance and a small electron density. A combination of both the $Se\cdots H$ hydrogen bond and the $X\cdots F$ interaction is responsible for the stability of the cyclic structure of $F_2CSe-HOX-I$, characterized with a ring critical point in Fig. 4. The presence of $X\cdots F$ interaction in $F_2CSe-HOX-I$ can be understood with the MEPs of HOX and F_2CSe . One can see from Fig. 1 that both F atoms of F_2CSe have positive MEPs near the region of the π -hole. As a result, the lone-pair electron of X atom in HOX is close to the F atom of F_2CSe . Furthermore, with the increase of X atomic mass, the deviation of X-O bond from the molecular plane of F_2CSe becomes larger, shown in Fig. S1. The nonplanar structure of $F_2CSe-HOX-I$ is different from the planar structure of hydrogen-bonded complexes of $H_2CO-HOX^{18}$ and $H_2CS-HOX^{35}$, where the X atom approaches the H atom of H_2CY (Y = O and S) with a weak $H\cdots X$ interaction.

In $F_2CSe-HOX-II$, the lone-pair electron on the oxygen atom of HOX attacks the π -hole of F_2CSe , forming a tetrel-bonded complex. The tetrel bond is an attractive interaction between a positive region of MEP adjoined with the IV group atom and a Lewis base.³⁶⁻³⁹ The acidic H atom of HOX is located between two F atoms of F_2CSe , while the X atom deviates from the C=Se axis. As shown in Fig. S1, this deviation grows up with the increase of X atomic mass. It is interesting to find a $Se\cdots X$ BCP in $F_2CSe-HOBr-II$ and $F_2CSe-HOI-II$ complexes, which can be explained with the MEPs of HOX and F_2CSe . It is found from Fig. 1 that the C=Se bond has positive MEPs in the vertical direction to the molecular plane of F_2CSe . To confirm this $Se\cdots X$

interaction, we also perform an orbital interaction analysis for this type of complex. The results show that there is an orbital interaction of $Lp_X \rightarrow BD^*_{C-Se}$, where Lp_X and BD^*_{C-Se} are the lone-pair orbital of X atom and the anti-bonding orbital of C-Se bond, respectively. The corresponding second-order perturbation energy is 0.46 kJ/mol in the HOCl complex, 2.88 kJ/mol in the HOBr complex and 5.43 kJ/mol in the HOI complex. Clearly, the $Se \cdots X$ interaction becomes stronger with the increase of X atomic mass. Besides, the $C \cdots O$ distance is decreased following the same growth sequence, showing a consistent change with the negative MEP on the oxygen atom in HOX (Table 1) and the electron density at the $C \cdots O$ BCP (Fig. 4). The results indicate that the tetrel bond becomes stronger with the increase of X atomic mass.

In $F_2CSe-HOX-III$, the lone-pair electron of O atom in HOX is associated with the σ -hole on the Se atom, forming a chalcogen bond. The chalcogen bond is an attractive interaction between the σ -hole on the V group atom and a Lewis base.⁴⁰⁻⁴² $F_2CSe-HOX-III$ is a planar structure with Cs symmetry for most complexes except the HOI complex. The planar structure of HOI complex is unstable with one imaginary frequency. Likely, the chalcogen bond is also stronger with the increase of X atomic mass, confirmed by the shorter $Se \cdots O$ distance (Fig. 1), the more negative MEP on the oxygen atom in HOX (Table 1), and the bigger electron density at the $Se \cdots O$ BCP (Fig. 4). In $F_2CSe-HOX-IV$, a halogen bond is formed between the σ -hole of the halogen atom and the lone-pair electron on the Se atom for most complexes except the HOF complex. This is consistent with the fact that F atom seldom participates in halogen bond.⁴³ In the initial optimization of configuration IV, the HOX molecule is in a plane

with the F_2CSe molecule. However, in the final optimized structure, the H-O bond is almost perpendicular to the molecular plane of F_2CSe . This is also different from the planar structure of halogen-bonded complexes of $H_2CO-HOX$ ¹⁸ and $H_2CS-HOX$,³⁵ where the H atom of HOX is opposite to the H atom of H_2CY (Y = O and S).

Hypohalous acids have been studied both experimentally⁴⁴⁻⁴⁷ and theoretically⁴⁸⁻⁵⁰. Alkorta et al.³⁴ pointed out that the geometries of hypohalous acids at the MP2/aug'-cc-pVTZ level are in good agreement with the experimental results. The geometrical parameters of HOX obtained at the MP2/aug-cc-pVTZ level, including bond lengths and H-O-X angles, are also close to the experimental values. For instance, the experimental value of Br-O bond length in HOBr is 1.828 Å⁴⁴ and the corresponding theoretical value is 1.824 Å.

Table 2 presents the changes of H-O and X-O bond lengths in the complexes. Upon the formation of configurations I, II, and III, the H-O bond is elongated and its elongation is larger in the configuration I. However, the X-O bond shows an irregular change in three configurations. In I, the X-O bond is elongated in $F_2CSe-HOF$ complex but is contracted in other complexes. The change of X-O bond length in II and III is very small. In IV, the associated X-O bond is lengthened and the distant H-O bond displays a tiny contraction. The elongation of associated X-O bond is related to the interaction strength.

The frequency shifts of stretch vibrations for the H-O and X-O bonds are also listed in Table 2. In general, these shifts are consistent with the change of the respective bond length. In I, the associated H-O stretch vibration exhibits a large red

shift, varying from -169.0 to -197.1 cm^{-1} , while the X-O stretch vibration has a small blue shift. In II and III, a small shift is found for the stretch vibrations of the H-O and X-O bonds. As expected, the associated X-O bond also displays a red shift in IV, although its shift is smaller than that of the H-O bond in I. The distant H-O bond in IV shows a small blue shift, and this phenomenon was also observed in the other halogen-bonded complexes of HOX.^{18,35}

3.3. Interaction energies

Table 3 presents the interaction energies of the complexes at the MP2/aug-cc-pVTZ and CCSD(T)/aug-cc-pVTZ levels. The CCSD(T) values are obtained with a single-point energy calculation at the CCSD(T) level on the MP2 geometry. Both types of interaction energies are corrected for BSSE. As expected, the MP2 method overestimates the interaction energy relative to the CCSD(T) result. For the same type of complex, this overestimation is expanded with the increase of X atomic mass. The relative deviation is less than 30% in I, II, and III complexes but varies from 35% to 50% in IV. Obviously, the calculation method exerts the smallest effect on the interaction energy of F₂CSe-HOX-I complex, has a similar effect on the interaction energies of F₂CSe-HOX-II and F₂CSe-HOX-III complexes, and imposes the largest influence on the interaction energy of F₂CSe-HOX-IV complex. Even so, the changes of interaction energies are almost similar at both levels of theory. The following discuss is based on the MP2 interaction energies.

The relative stability of complex depends on the nature of X atom. For the F complexes, F₂CSe-HOF-I is the most stable, followed by F₂CSe-HOF-II, and

F₂CSe-HOF-III is the weakest. For the Cl complexes, they become more stable in order of III < IV ≈ II < I. For the Br complexes, F₂CSe-HOBr-IV is more stable than F₂CSe-HOBr-II, both of them being less stable than F₂CSe-HOBr-I. For the I complexes, F₂CSe-HOI-IV exhibits larger stability than F₂CSe-HOI-I, and the relative stability of II and III is similar to that in the Br counterpart. Clearly, the chalcogen-bonded complexes are the most unstable. The tetrel-bonded complex is more stable than the chalcogen-bonded one, consistent with the positive MEP on the π -hole and σ -hole in F₂CSe. For the tetrel- and chalcogen-bonded complexes, the interaction energy shows a consistent change with the binding distance. That is, the bigger interaction energy corresponds to the shorter binding distance. Of course, there is little difference in stability for the four structures, thus a competition occurs between them.

It was demonstrated that HOX can form a hydrogen bond and a halogen bond with H₂CO, and the hydrogen bond is stronger than the halogen bond although their difference in stability is reduced with the increase of X atomic mass.¹⁸ This conclusion still holds in the complexes of HOX and F₂CSe when X is F, Cl, and Br. For HOI, however, the halogen bond is stronger than the hydrogen bond in the F₂CSe complex despite the existence of both a Se...H hydrogen bond and a F...I interaction in F₂CSe-HOI-I. Actually, the interaction energy of Se...H hydrogen bond is smaller than -17.5 kJ/mol if the F...I interaction is deleted from F₂CSe-HOI-I. Due to this reason, the interaction energy of F₂CSe-HOX-I does not accurately reflect the strength of Se...H hydrogen bond, which can be estimated with the binding distance. However,

the strength of halogen bond is not measured with the binding distance due to the different halogen atom.

3.4. NBO analysis

To unveil the formation mechanism of these complexes, we performed a NBO analysis for them. Charge transfer and second-order perturbation energy are given in Table 4. A charge transfer occurs between the two molecules in all complexes. Generally, the charge transfer shows a consistent change with the interaction energy. This indicates that the charge transfer interaction plays an important role in the formation of these complexes. The magnitude of charge transfer is small in the tetrel- and chalcogen-bonded complexes, showing the minor contribution of charge transfer. The charge transfer in $F_2CSe-HOX-I$ is larger than that of hydrogen-bonded complex of H_2CO and HOX ,¹⁸ although the interaction energy in the former is smaller than that in the latter. The possible reason is attributed to the nature of Se atom. This atom has a bigger atomic radius and a smaller electronegativity, thus it is easier to lose electrons. In addition, the change of charge transfer in $F_2CSe-HOX-I$ is not prominent with the increase of X atomic mass. The similar reason results in a big charge transfer in the halogen-bonded complexes of F_2CSe and HOX . Furthermore, the charge transfer in the halogen-bonded complexes is changed significantly with the increase of X atomic mass. For instance, it varies from 0.0244e in $F_2CSe-HOCl-IV$ to 0.0808e in $F_2CSe-HOI-IV$. A comparative analysis indicates that the value of charge transfer is small for the complexes with Se as the Lewis acid but is large for the complexes with Se as the Lewis base.

The $F_2CSe-HOX-I$ complex is analyzed with three orbital interactions of $BD_{C-Se} \rightarrow BD_{O-H}^*$, $Lp_{Se} \rightarrow BD_{O-H}^*$ and $BD_{O-X} \rightarrow RY_F^*$. The first two orbital interactions correspond to the formation of $Se \cdots H$ hydrogen bond, while the third one is connected with the $X \cdots F$ interaction. One can see in Table 5 that the first two orbital interactions are much stronger than the third one. This means that the hydrogen bond has a dominant contribution to the stability of $F_2CSe-HOX-I$ complex and the $X \cdots F$ interaction plays a minor stabilizing role. In the formation of hydrogen bond, the orbital interaction between the $C=Se$ bond orbital and the $H-O$ anti-bonding orbital is dominant in the complexes of HOX ($X = F, Cl, \text{ and } Br$), whereas the orbital interaction between the lone-pair orbital of Se and the $H-O$ anti-bonding orbital is mainly responsible for it in $F_2CSe-HOI-I$. The former orbital interaction is different from that in the hydrogen-bonded complexes of $H_2CO-HOX$ ¹⁸ and $H_2CS-HOX$,³⁵ where $Lp_{O(S)} \rightarrow BD_{O-H}^*$ is the dominant orbital interaction. With the increase of X atomic mass, the $BD_{O-X} \rightarrow RY_F^*$ orbital interaction becomes bigger, indicating the stronger $X \cdots F$ interaction.

Both types of orbital interactions ($Lp_O \rightarrow BD_{C-Se}^*$ and $Lp_X \rightarrow BD_{C-Se}^*$) have been analyzed for the $F_2CSe-HOX-II$ complex. The former orbital interaction is related to the formation of tetrel bond, while the latter one is involved in the $X \cdots Se$ interaction. Obviously, the $F_2CSe-HOX-II$ complex is mainly stabilized by the tetrel bond, and the secondary $X \cdots Se$ interaction has small contribution to its conformation. Likely, the $Lp_O \rightarrow BD_{C-Se}^*$ orbital interaction is a main orbital interaction in the chalcogen-bonded complexes. For the nonplanar $F_2CSe-HOI-III$ complex, another orbital interaction of

$Lp_I \rightarrow BD^*_{C-Se}$ also has a comparable contribution to its stability with the $Lp_O \rightarrow BD^*_{C-Se}$ orbital interaction. The above orbital interactions confirm the weak interactions in II and III.

There are two main orbital interactions in the halogen-bonded complexes. The dominant orbital interaction is $BD_{C-Se} \rightarrow BD^*_{Cl-O}$ in $F_2CSe-HOCl-IV$ but $Lp_{Se} \rightarrow BD^*_{X-O}$ in $F_2CSe-HOBr-IV$ and $F_2CSe-HOI-IV$, depending on the nature of HOX . The former orbital interaction is like that in $F_2CSe-HOX-I$ ($X = F, Cl, \text{ and } Br$). The corresponding perturbation energy is all larger than that of the $BD_{O-X} \rightarrow RY^*_{Se}$ orbital interaction. The large perturbation energy is consistent with the big charge transfer in the halogen-bonded complexes.

3.5. Electron density shifts

It has been demonstrated that total electron density maps can accurately determine electron density shifts,⁵¹ which are useful for detecting noncovalent interactions, particularly in complicated systems. The shifts that occur in all complexes are plotted in Fig. 5, where red and blue regions represent increased and decreased electron densities, respectively. These maps were generated by comparing the electron density in the complex to the sum of the electron densities of the isolated subsystems frozen in the optimized structure of the complex.

In general, there is a pattern commonality in all of these complexes. A red increase occurs on the electron donor atom such as the Se lone pair in the hydrogen and halogen bonds as well as the O lone pair in the tetrel and chalcogen bonds. Simultaneously, a blue area of charge loss is found in the acidic proton in the

hydrogen bond, the π -hole in the tetrel bond, the σ -hole on the Se atom in the chalcogen bond, and the σ -hole on the halogen atom in the halogen bond, respectively. Moreover, the magnitudes of these areas can be used to estimate the strength of the same type interaction. For instance, with the increase of X atomic mass, the contour near the σ -hole on the Se atom in the chalcogen bond is denser, consistent with the change of interaction strength. It is also found that the maps are more complicated with the increase of interaction strength and the presence of another secondary interaction.

3.6. Energy decomposition analysis

To unveil the nature of interactions in the complexes, the interaction energies are decomposed into three attractive terms of electrostatic (E^{ele}), polarization (E^{pol}), and dispersion (E^{disp}), gathered in Table 5. One can see that the electrostatic energy plays an important role in stabilizing most complexes except some weak complexes, where the dispersion energy is more important than the electrostatic energy or has a comparable contribution with the electrostatic energy. In the tetrel- and chalcogen-bonded complexes, the contribution of the polarization energy is much smaller than that from the electrostatic and dispersion energies.

With the increase of X atomic mass in the complex I, the contribution of electrostatic and polarization energies is decreased, while that of dispersion energy is increased. The electrostatic energy has a consistent change with the positive electrostatic potential on the H atom of HOX (Table 1), indicating that the electrostatic energy is mainly from the Se \cdots H hydrogen bond. The change of

dispersion energy is consistent with the strength of $X\cdots F$ interaction, showing the chief contribution of $X\cdots F$ interaction to the dispersion energy. Moreover, the contribution of dispersion energy shows a more prominent change than that of electrostatic energy. The reverse change of both electrostatic energy and dispersion energy is responsible for the small difference of the interaction energy in different complexes I.

With the increase of X atomic mass in IV, the contribution of polarization energy grows up, whereas that of dispersion energy is reduced, both of them are different from that in I. Although the values of three attractive terms are increased in IV with the increase of X atomic mass, the relative contribution of electrostatic energy is changed a little and the relative contribution of polarization and dispersion energies has a prominent change. Moreover, the relative contribution of polarization energy has a consistent change with the interaction energy. As a result, the polarization energy has a large contribution to the strength of halogen bond when the halogen atom is varied.

4. Conclusions

The complexes of F_2CSe and hypohalous acid HOX ($X = F, Cl, Br, \text{ and } I$) have been studied to identify local minima on the complex potential surface, to characterize the types of interactions, to evaluate their stabilization, and to unveil their formation mechanism. These calculations support the following conclusions.

(1) Four equilibrium structures have been found on the $F_2CSe-HOX$ ($X = F, Cl, Br, \text{ and } I$) potential surface except $F_2CSe-HOF$, in which three structures are found. These

complexes are mainly stabilized by a $\text{Se}\cdots\text{H}$ hydrogen bond (I), a $\pi\cdots\text{O}$ tetrel bond (II), a $\text{Se}\cdots\text{O}$ chalcogen bond (III), and a $\text{Se}\cdots\text{X}$ halogen bond (IV). A secondary $\text{X}\cdots\text{F}$ interaction coexists with the hydrogen bond in I and a $\text{Se}\cdots\text{X}$ interaction is also present in most II. Both secondary interactions in I and II become stronger with the increase of X atomic mass.

(2) The complex I is the most stable for HOX (X = F, Cl, and Br), showing a little dependence on the nature of X due to the coexistence of the $\text{Se}\cdots\text{H}$ hydrogen bond and the $\text{X}\cdots\text{F}$ interaction. For HOI, the complex IV is more stable than the complex I. With the increase of X atomic mass, the complexes II, III and IV become more stable. The chalcogen bond is weakest, and the tetrel bond is stronger than the chalcogen bond.

(3) In I, the associated H-O bond is elongated and shows a large red shift, while the X-O has a small change. In IV, the X-O bond is also lengthened but has a small red shift, while the distant H-O bond displays a small blue shift. The changes of H-O and X-O bonds are negligible in II and III.

(4) In I, the $\text{BD}_{\text{C-Se}}\rightarrow\text{BD}_{\text{H-O}}^*$ orbital interaction is dominant in the hydrogen bond of HOX (X = F, Cl, and Br), while the $\text{Lp}_{\text{Se}}\rightarrow\text{BD}_{\text{H-O}}^*$ one plays a main role in the hydrogen bond of HOI. The $\text{Lp}_{\text{O}}\rightarrow\text{BD}_{\text{C-Se}}^*$ orbital interaction has a major contribution to the formation of tetrel and chalcogen bonds although the $\text{Lp}_{\text{I}}\rightarrow\text{BD}_{\text{C-Se}}^*$ one is also important in $\text{F}_2\text{CSe-HOI-III}$. For the halogen bond, the $\text{BD}_{\text{C-Se}}\rightarrow\text{BD}_{\text{Cl-O}}^*$ orbital interaction is dominant for HOCl, while the $\text{Lp}_{\text{Se}}\rightarrow\text{BD}_{\text{X-O}}^*$ one is principal for HOBr and HOI.

(5) The electrostatic energy is dominant in the Se...H hydrogen bond, while the X...F interaction in I is dominated by the dispersion energy. The dispersion energy is comparable with the electrostatic energy in the tetrel and chalcogen bonds. The electrostatic energy is also principal attractive force in the halogen bond, but the polarization energy has major responsibility for the change of its interaction energy with HOX.

Acknowledgements

This work was supported by the Outstanding Youth Natural Science Foundation of Shandong Province (JQ201006), the Key Project of Natural Science Foundation of Shandong Province of China (ZR2013HZ004), and the Graduate Innovation Foundation of Yantai University (YJSZ201509).

References

- 1 H. Y. Liao, M. D. Su and S. Y. Chu, *J. Chem. Phys.*, 2000, **261**, 275-287.
- 2 J. S. Kwiatkowski and J. Leszczyski, *Mol Phys.*, 1993, **97**, 1845-1849.
- 3 J. S. Kwiatkowski and J. Leszczyski, *Mol Phys.*, 1994, **81**, 119-131.
- 4 J. S. Kwiatkowski and B. Pullman, *Adv. Heterocyclic Chem.*, 1975, **18**, 199-335.
- 5 J. G. Melnick, K. Yurkerwich and G. Parkin, *J. Am. Chem. Soc.*, 2010, **132**, 647-655.
- 6 R. Butler and A. Snelson, *J. Phys. Chem.*, 1979, **83**, 3243-3248.
- 7 A. Böck, K. Forchhammer, J. Heider, W. Leinfelder, G. Sawers, B. Veprek and F. Zinoni, *Mol. Microbiol.*, 1991, **3**, 515-520.
- 8 G. M. Li, M. Segi and T. Nakajima, *Tetrahed. Lett.*, 1992, **33**, 3515-3518.

- 9 S. M. Bachrach and S. L. Jiang, *J. Org. Chem.*, 1999, **64**, 8248-8255.
- 10 M. Y. Boluk, D. C. Moule and D. J. Clouthier, *Can. J. Chem.*, 1983, **61**, 1743-1748.
- 11 R. H. Judge and D. C. Moule, *J. Am. Chem. Soc.*, 1984, **106**, 5406-5407.
- 12 H. Bock, S. Aygen, P. Rosmus, B. Solouki and E. Weissflog, *Chem. Ber.*, 1984, **117**, 187-201.
- 13 M. Solimannejad, I. Alkorta and J. Elguero, *Chem. Phys. Lett.*, 2008, **454**, 201-206.
- 14 M. Solimannejad and S. Scheiner, *J. Phys. Chem. A*, 2008, *112*, 4120-4124.
- 15 M. Solimannejad, I. Alkorta and J. Elguero, *Chem. Phys. Lett.*, 2007, **449**, 23-27.
- 16 M. Solimannejad and L. Pejov, *J. Phys. Chem. A*, 2005, **109**, 825-831.
- 17 A. F. Jalbout, X. H. Li and M. Solimannejad, *Chem. Phys. Lett.*, 2006, **420**, 204-208.
- 18 Q. Z. Li, X. S. Xu, T. Liu, B. Jing, W. Z. Li, J. B. Cheng, B. A. Gong and J. Z. Sun, *Phys. Chem. Chem. Phys.*, 2010, **12**, 6837-6843.
- 19 R. R. Garcia and S. Solomon, *J. Geophys. Res.*, 1994, **99**, 12937-12951.
- 20 X. H. Cheng, H. Z. Jia, T. Long, J. Feng, J. G. Qin and Z. Li, *Chem. Commun.*, 2011, **47**, 11978-11980.
- 21 H. M. Abu-Soud, D. Maitra, J. Byun, C. E. A. Souza, J. Banerjee, G. M. Saed, M. P. Diamond, P. R. Andreana and S. Pennathur, *Free Radical Biol. Med.*, 2012, **52**, 616-625.
- 22 Z. Prokopowicz, J. Marcinkiewicz, D. R. Katz and B. M. Chain, *Arch. Immunol.*

- Ther. Exp.*, 2012, **60**, 43-54.
- 23 Y. C. Yang, H. H. Lu, W. T. Wang and L. Liao, *Anal. Chem.*, 2011, **83**, 8267-8272.
- 24 S. F. Boys and F. Bernardi, *Mol. Phys.*, 1970, **19**, 553-556.
- 25 M. J. Frisch, G. W. Trucks, H. B. Schlegel, G. E. Scuseria, M. A. Robb, J. R. Cheeseman, J. A. Montgomery, Jr, T. Vreven, K. N. Kudin, J. C. Burant, J. M. Millam, S. S. Iyengar, J. Tomasi, V. Barone, B. Mennucci, M. Cossi, G. Scalmani, N. Rega, G. A. Petersson, H. Nakatsuji, M. Hada, M. Ehara, K. Toyota, R. Fukuda, J. Hasegawa, M. Ishida, T. Nakajima, Y. Honda, O. Kitao, H. Nakai, M. Klene, X. Li, J. E. Knox, H. P. Hratchian, J. B. Cross, C. Adamo, J. Jaramillo, R. Gomperts, R. E. Stratmann, O. Yazyev, A. J. Austin, R. Cammi, C. Pomelli, J. W. Ochterski, P. Y. Ayala, K. Morokuma, G. A. Voth, P. Salvador, J. J. Dannenberg, V. G. Zakrzewski, S. Dapprich, A. D. Daniels, M. C. Strain, O. Farkas, D. K. Malick, A. D. Rabuck, K. Raghavachari, J. B. Foresman, J. V. Ortiz, Q. Cui, A. G. Baboul, S. Clifford, J. Cioslowski, B. B. Stefanov, G. Liu, A. Liashenko, P. Piskorz, I. Komaromi, R. L. Martin, D. J. Fox, T. Keith, M. A. Al Laham, C. Y. Peng, A. Nanayakkara, M. Challacombe, P. M. W. Gill, B. Johnson, W. Chen, M. W. Wong, C. Gonzalez and J. A. Pople, *Gaussian 09, Revision A.02*, Gaussian, Inc., Wallingford CT, 2009.
- 26 F. A. Bulat, A. Toro-Labbe, T. Brinck, J. S. Murray and P. Politzer, *J. Mol. Model.*, 2010, **16**, 1679-1691.
- 27 R. F. W. Bader, *AIM2000 Program, v. 2.0*, McMaster University, Hamilton,

- Canada, 2000.
- 28 T. Lu and F. Chen, *J. Comput. Chem.*, 2012, **33**, 580-592.
- 29 A. E. Reed, L. A. Curtiss and F. Weinhold, *Chem. Rev.*, 1988, **88**, 899-926.
- 30 P. F. Su and H. Li, *J. Chem. Phys.*, 2009, **13**, 014102.
- 31 M. W. Schmidt, K. K. Baldridge, J. A. Boatz, S. T. Elbert, M. S. Gordon, J. H. Jensen, S. Koseki, N. Matsunaga, K. A. Nguyen, S. J. Su, T. L. Windus, M. Dupuis and J. A. Montgomery, *J. Comput. Chem.*, 1993, **14**, 1347-1363.
- 32 X. Guo, X. L. An and Q. Z. Li, *J. Phys. Chem. A*, 2015, **119**, 3518-3527.
- 33 G. Sanchez-Sanz, C. Trujillo, I. Alkorta and J. Elguero, *Phys. Chem. Chem. Phys.*, 2012, **14**, 9880-9889.
- 34 I. Alkorta, F. Blanco, M. Solimannejad and J. Elguero, *J. Phys. Chem. A*, 2008, **112**, 10856-10863.
- 35 Q. Z. Li, B. Jing, R. Li, Z. B. Liu, W. Z. Li, F. Luan, J. B. Cheng, B. A. Gong and J. Z. Sun, *Phys. Chem. Chem. Phys.*, 2011, **13**, 2266-2271.
- 36 A. Bauzá, T. J. Mooibroek and A. Frontera, *Angew. Chem. Int. Ed.*, 2013, **125**, 12543-12547.
- 37 Q. Z. Li, X. Guo, X. Yang, W. Z. Li, J. B. Cheng and H. B. Li, *Phys. Chem. Chem. Phys.*, 2014, **16**, 11617-11625.
- 38 D. Mani and E. Arunan, *J. Phys. Chem. A*, 2014, **118**, 10081-10089.
- 39 Q. Z. Li, H. Y. Zhuo, H. B. Li, Z. B. Liu, W. Z. Li and J. B. Cheng, *J. Phys. Chem. A*, 2015, **119**, 2217-2224.
- 40 W. Wang, B. Ji and Y. Zhang, *J. Phys. Chem. A*, 2009, **113**, 8132-8135.

- 41 Q. Z. Li, H. Qi, R. Li, X. F. Liu, W. Z. Li and J. B. Cheng, *Phys. Chem. Chem. Phys.*, 2012, **14**, 3025-3030.
- 42 Q. Zhao, D. C. Feng, Y. M. Sun, J. C. Hao and Z.T. Cai, *Int. J. Quantum Chem.*, 2011, **111**, 3881-3887.
- 43 P. Politzer, J. S. Murray and T. Clark, *Phys. Chem. Chem. Phys.*, 2010, **12**, 7748-7757.
- 44 A. Callegari, P. Theule, R. Schmied, T. R. Rizzo and J. S. Muentner, *J. Mol. Spectrosc.*, 2003, **221**, 116-120.
- 45 D. R. Hanson and E. R. Lovejoy, *J. Phys. Chem.*, 1996, **100**, 6397-6405.
- 46 R. J. Barnes, M. Lock, J. Coleman and A. Sinha, *J. Phys. Chem.*, 1996, **100**, 453-457.
- 47 M. Lock, R. J. Barnes, and A. Sinha, *J. Phys. Chem.*, 1996, **100**, 7972-7980.
- 48 R. M. Escibano, G. D. Lonardo and L. Fusina, *Chem. Phys. Lett.*, 1996, **259**, 614-618 ,
- 49 P. Burk, I. A. Koppel, A. Rummel and A. Trummal, *J. Phys. Chem.*, 1995, **99**, 1432-1435.
- 50 J. A. Pople and L. A. Curtiss, *J. Chem. Phys.*, 1989, **90**, 2833.
- 51 S. Scheiner and T. Kar, *J. Phys. Chem. A*, 2002, **106**, 1784-1789.

Figure captions

Fig. 1 MEPs of F₂CSe. Color ranges, in eV, are: red, greater than 0.27; yellow, between 0.27 and 0; blue, less than 0

Fig. 2 MEPs of HOX (X = F, Cl, Br, and I). Color ranges, in eV, are: red, greater than 0.27; yellow, between 0.27 and 0; blue, less than 0

Fig. 3 Optimized structures of the complexes with distances (Å)

Fig. 4 Molecular graphs of all complexes with bond critical points (red points) and ring critical points (yellow points)

Fig. 5 Electron density shifts maps of all complexes. Red and blue lines represent the increased and decreased electron densities, respectively. Contours are shown at the 0.0012 au level.

Fig. 1

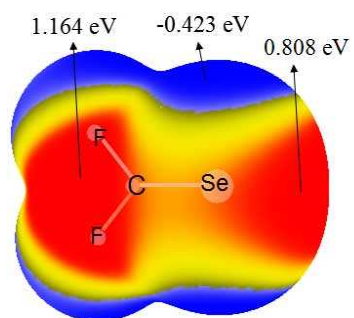


Fig. 2

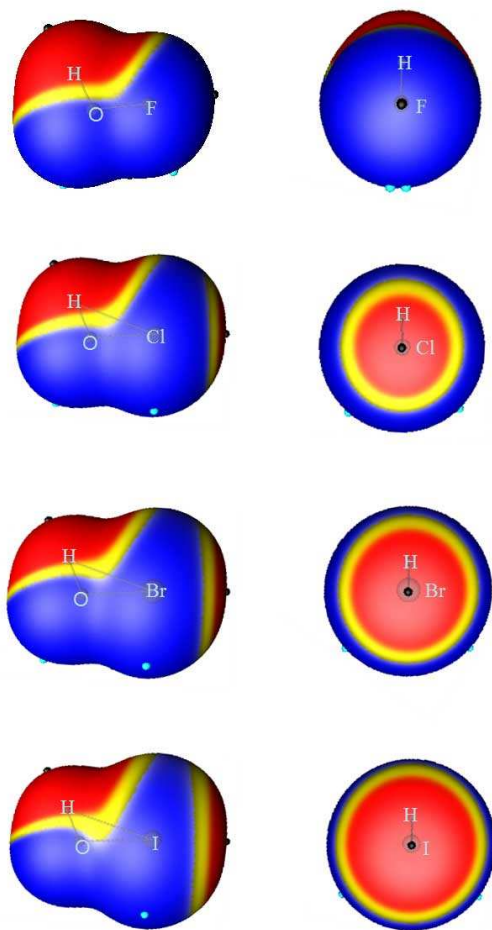


Fig. 3

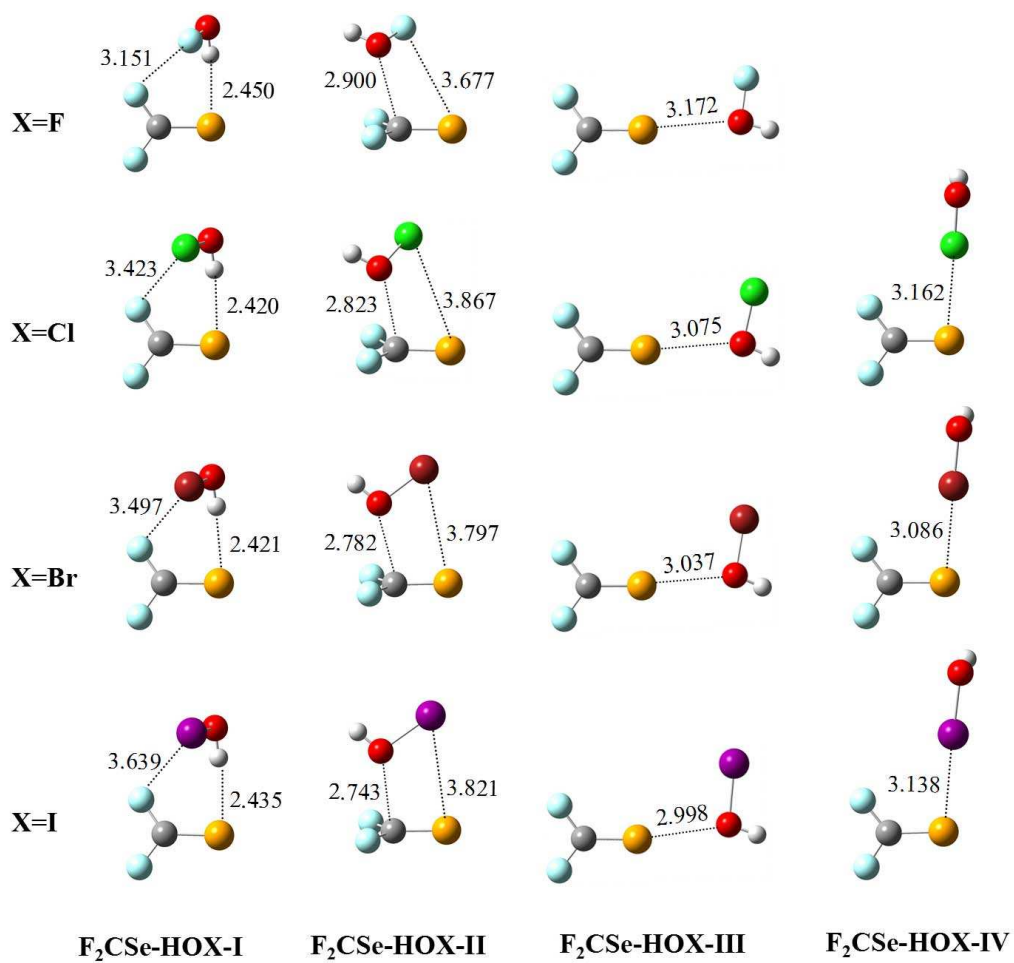


Fig. 4

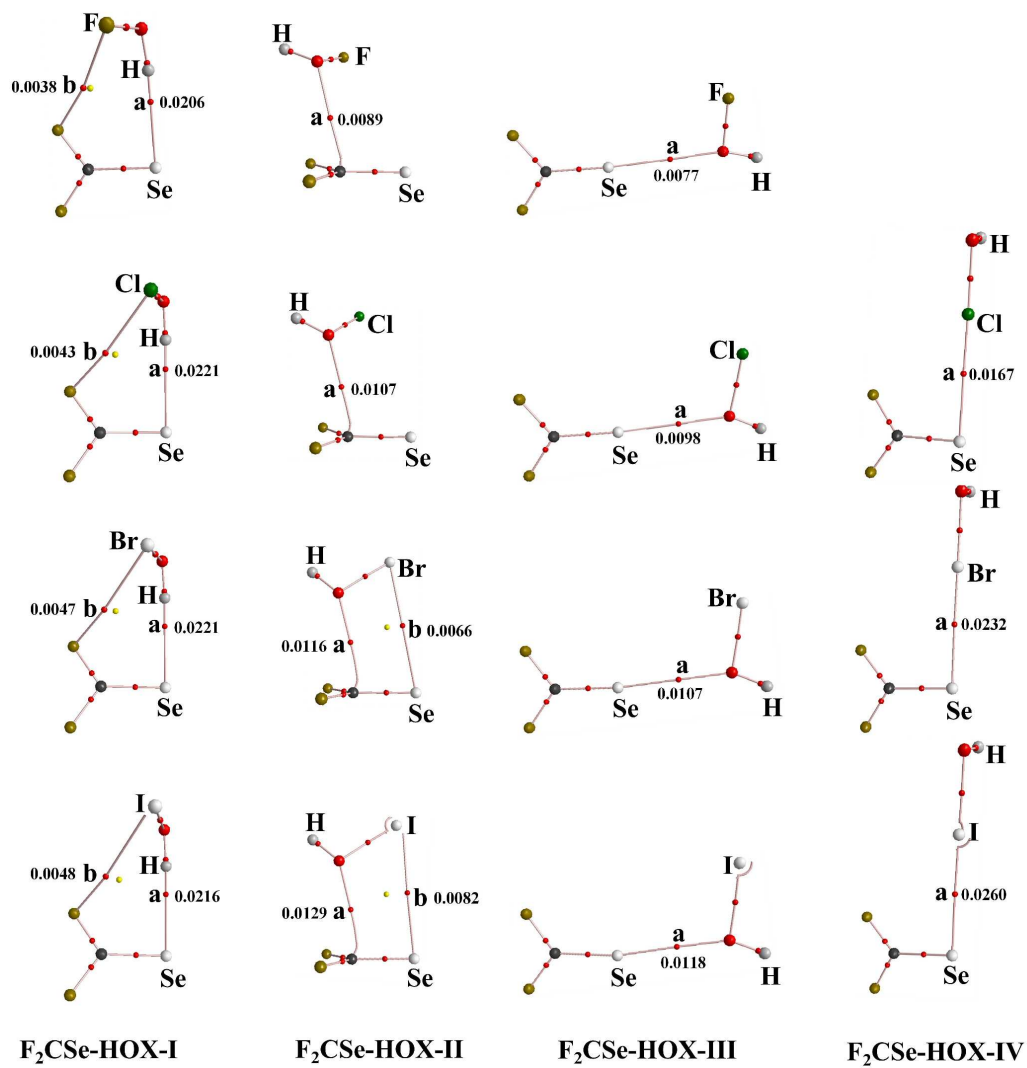


Fig. 5

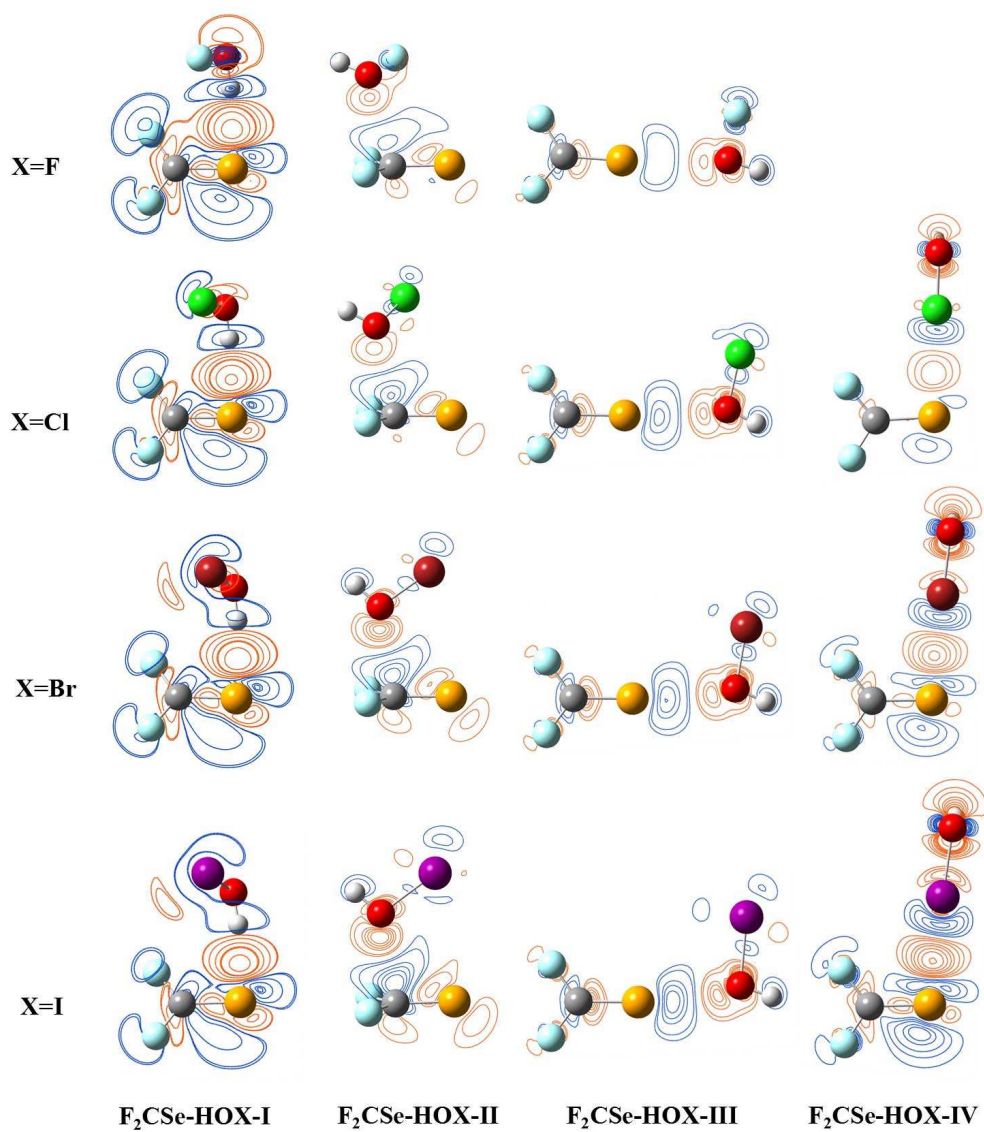


Table 1 The most positive (V_{\max}) and negative (V_{\min}) MEPs in HOX (X = F, Cl, Br, and I). All are in eV

Monomer	$V_{\max}(\text{H})$	$V_{\max}(\text{X})$	$V_{\min}(\text{X})$	$V_{\min}(\text{O})$
HOF	2.592	---	-0.675	-0.744
HOCl	2.427	1.035	-0.406	-0.817
HOBr	2.329	1.358	-0.339	-0.868
HOI	2.202	1.716	-0.261	-0.950

Table 2 Changes of bond lengths (Δr , Å) and frequency shifts ($\Delta \nu$, cm^{-1}) of H-O and x-O bonds in the complexes at the MP2/aug-cc-pVTZ level

Complexes	$\Delta r_{\text{H-O}}$	$\Delta r_{\text{X-O}}$	$\Delta \nu_{\text{H-O}}$	$\Delta \nu_{\text{X-O}}$
F ₂ CSe-HOF-I	0.008	0.002	-169.0	1.7
F ₂ CSe-HOCl-I	0.010	-0.003	-197.1	3.4
F ₂ CSe-HOBr-I	0.009	-0.005	-196.3	5.5
F ₂ CSe-HOI-I	0.009	-0.006	-186.1	5.1
F ₂ CSe-HOF-II	0.001	0.000	-9.1	-3.0
F ₂ CSe-HOCl-II	0.001	0.001	-9.0	-1.8
F ₂ CSe-HOBr-II	0.001	-0.000	-8.9	2.0
F ₂ CSe-HOI-II	0.001	-0.000	-9.7	3.4
F ₂ CSe-HOF-III	0.001	-0.001	-5.7	-0.5
F ₂ CSe-HOCl-III	0.001	0.001	-5.7	-1.6
F ₂ CSe-HOBr-III	0.001	0.001	-6.7	-0.5
F ₂ CSe-HOI-III	0.001	0.002	-6.5	-2.0
F ₂ CSe-HOCl-IV	-0.000	0.013	1.8	-39.7
F ₂ CSe-HOBr-IV	-0.000	0.021	3.0	-46.9
F ₂ CSe-HOI-IV	-0.001	0.022	10.8	-37.4

Table 3 Interaction energies corrected for BSSE (ΔE , kJ/mol) at the MP2/aug-cc-pVTZ and CCSD(T)/aug-cc-pVTZ levels

Complexes	ΔE^{MP2}	$\Delta E^{\text{CCSD(T)}}$
F ₂ CSe-HOF-I	-14.4	-14.6
F ₂ CSe-HOCl-I	-17.2	-15.5
F ₂ CSe-HOBr-I	-17.4	-15.2
F ₂ CSe-HOI-I	-17.5	-14.7
F ₂ CSe-HOF-II	-7.3	-6.5
F ₂ CSe-HOCl-II	-10.5	-8.5
F ₂ CSe-HOBr-II	-11.6	-9.0
F ₂ CSe-HOI-II	-13.3	-10.2
F ₂ CSe-HOF-III	-4.8	-4.2
F ₂ CSe-HOCl-III	-7.3	-6.0
F ₂ CSe-HOBr-III	-8.3	-6.6
F ₂ CSe-HOI-III	-9.6	-7.6
F ₂ CSe-HOCl-IV	-10.1	-6.8
F ₂ CSe-HOBr-IV	-15.7	-10.7
F ₂ CSe-HOI-IV	-22.1	-16.3

Table 4 Charge transfer (CT , e) and second-order perturbation energy (E^2 , kJ/mol) in the complexes at the HF/aug-cc-pVTZ level

Complexes	CT	E_1^2	E_2^2	E_3^2
F ₂ CSe-HOF-I	0.0274	47.6	6.0	0.6
F ₂ CSe-HOCl-I	0.0286	51.1	6.8	2.5
F ₂ CSe-HOBr-I	0.0278	48.9	6.3	2.9
F ₂ CSe-HOI-I	0.0251	0.3	46.3	3.2
F ₂ CSe-HOF-II	0.0054	8.2	---	---
F ₂ CSe-HOCl-II	0.0075	10.2	0.46	---
F ₂ CSe-HOBr-II	0.0083	11.2	2.88	---
F ₂ CSe-HOI-II	0.0094	12.5	5.43	---
F ₂ CSe-HOF-III	0.0031	7.5	---	---
F ₂ CSe-HOCl-III	0.0041	8.7	---	---
F ₂ CSe-HOBr-III	0.0039	9.7	---	---
F ₂ CSe-HOI-III	0.0094	11.4	7.6	---
F ₂ CSe-HOCl-IV	0.0244	28.7	9.3	---
F ₂ CSe-HOBr-IV	0.0544	78.0	9.9	---
F ₂ CSe-HOI-IV	0.0808	117.1	7.2	----

Note: E_1^2 is the stabilization energy due to the orbital interaction of $BD_{C-Se} \rightarrow BD_{H-O}^*$ in I, $Lp_O \rightarrow BD_{C-Se}^*$ in II and III, $BD_{C-Se} \rightarrow BD_{Cl-O}^*$ in F₂CSe-HOCl-IV, and $Lp_{Se} \rightarrow BD_{X-O}^*$ in other IV. E_2^2 denotes the orbital interactions of $Lp_{Se} \rightarrow BD_{H-O}^*$ in I, $Lp_X \rightarrow BD_{C-Se}^*$ in II and III, and $BD_{O-X} \rightarrow RY_{Se}^*$ in IV. E_3^2 denotes the orbital interaction of $BD_{O-X} \rightarrow RY_F^*$ in I. The charge transfer is the absolute value of the sum of charge on all atoms of F₂CSe in the complexes.

Table 5 Electrostatic energy (E^{ele}), polarization energy (E^{pol}), dispersion energy (E^{disp}), exchange and repulsion energy ($E^{\text{ex+rep}}$), and interaction energy (E_{int}) in the complexes at the MP2/aug-cc-pVTZ level. All are in kJ/mol

Complexes	E^{ele}	E^{pol}	E^{disp}	$E^{\text{ex+rep}}$	E_{int}
F ₂ CSe-HOF-I	-23.9(48.6%)	-15.5(31.5%)	-9.8(19.9%)	34.6	-14.5
F ₂ CSe-HOCl-I	-26.4(44.1%)	-15.9(26.6%)	-17.5(29.3%)	42.4	-17.4
F ₂ CSe-HOBr-I	-27.4(43.7%)	-15.7(25.0%)	-19.6(31.3%)	45.5	-17.3
F ₂ CSe-HOI-I	-28.1(42.9%)	-15.1(23.1%)	-22.3(34.0%)	48.3	-17.1
F ₂ CSe-HOF-II	-10.1(44.1%)	-2.4(10.5%)	-10.4(45.4%)	15.6	-7.2
F ₂ CSe-HOCl-II	-15.5(45.3%)	-3.7(10.8%)	-15.0(43.9%)	24.0	-10.3
F ₂ CSe-HOBr-II	-20.6(48.1%)	-5.3(12.4%)	-16.9(39.5%)	31.4	-11.3
F ₂ CSe-HOI-II	-27.0(49.5%)	-8.1(14.8%)	-19.5(35.7%)	41.9	-12.7
F ₂ CSe-HOF-III	-5.3(36.3%)	-1.8(12.3%)	-7.5(51.4%)	8.4	-6.1
F ₂ CSe-HOCl-III	-8.7(42.2%)	-2.3(11.2%)	-9.6(46.6%)	13.4	-7.3
F ₂ CSe-HOBr-III	-10.7(43.3%)	-2.9(11.7%)	-11.1(44.9%)	16.4	-8.2
F ₂ CSe-HOI-III	-14.2(45.4%)	-4.0(12.8%)	-13.1(41.9%)	21.9	-9.4
F ₂ CSe-HOCl-IV	-26.8(44.7%)	-13.3(22.2%)	-19.9(33.2%)	49.5	-10.4
F ₂ CSe-HOBr-IV	-49.4(47.9%)	-26.7(25.9%)	-27.0(26.2%)	87.1	-15.9
F ₂ CSe-HOI-IV	-60.7(46.5%)	-41.3(31.6%)	-28.5(21.8%)	108.4	-22.0

Note: Data in parentheses are the percentage of each term to the sum of the three attractive energies.